Crossover of the intrinsic spin Hall effect in the presence of lattice expansion

Nozomi Soya,[1] Hiroki Hayashi,[1] Takashi Harumoto,[2] Tenghua Gao,[1,3] Satoshi Haku,[1] and Kazuya Ando[1,3,4,*]

[1]*Department of Applied Physics and Physico-Informatics, Keio University, Yokohama 223-8522, Japan*

[2]*School of Materials and Chemical Technology, Tokyo Institute of Technology, Tokyo 152-8552, Japan*

[3]*Keio Institute of Pure and Applied Sciences, Keio University, Yokohama 223-8522, Japan*

[4]*Center for Spintronics Research Network, Keio University, Yokohama 223-8522, Japan*

(Received 29 January 2021; revised 21 April 2021; accepted 6 May 2021; published 24 May 2021)

We report the robustness of the intrinsic spin Hall effect in Pt against a change in the lattice constant. We measure spin-torque ferromagnetic resonance for $Pt/Ni_{81}Fe_{19}$ bilayers, where the lattice constant and carrier scattering time of the Pt layer are varied by incorporating the nitrogen atoms as interstitial impurities. We find that the spin Hall angle is enhanced by a factor of 3 as the resistivity of the Pt layer is increased by the nitrogen incorporation. The variation of the spin Hall conductivity is consistent with the prediction of the crossover of the intrinsic spin Hall effect from the moderately dirty regime to the dirty-metal regime. This result demonstrates the variation of the intrinsic spin Hall conductivity in Pt is dominated by the change in the scattering time, rather than the change in the band structure, under a few percent change in the lattice constant.

DOI: 10.1103/PhysRevB.103.174427

I. INTRODUCTION

The spin Hall effect and its inverse effect have played a crucial role in exploring the physics of spin currents in condensed matter [1–9]. The spin Hall effect converts an applied charge current into a spin current through the spin-orbit coupling, enabling electric generation of a spin current in a variety of materials [10,11]. The spin current originating from the spin Hall effect can be injected into an adjacent ferromagnetic layer. This process transfers the angular momentum from the spin current to the local magnetic moments, exerting torques on the magnetization, which are called spin-orbit torques [12–27]. The current-induced spin-orbit torques provide a way for electrical manipulation of the magnetization, enabling us to induce magnetization precession, domain-wall motion, and magnetization switching [15]. The manipulation of the magnetization using spin-orbit torques promises various concepts of spintronic devices based on the spin Hall effect, opening the field of spin-orbitronics.

Since the first observation of the spin Hall effect more than a decade ago, diverse studies of the spin Hall effect in Pt have provided important information for the fundamental understanding of the conversion between spin and charge currents [28–41]; Pt has been central in establishing the spin-transport phenomena induced by the spin-orbit coupling. Previous studies have shown that the spin Hall effect can be tuned by changing the composition in Pt-based alloys [34–37], which provides a way to enhance the spin Hall conductivity. It has also been demonstrated that the spin Hall effect in Pt can be manipulated by varying the carrier scattering time by doping impurities, as well as changing the deposition method and condition [29,38–40].

The previous studies have shown that the spin Hall effect in Pt is dominated by the intrinsic mechanism. The intrinsic spin Hall effect originates from interband excitations between spin-orbit split bands [42]. In the intrinsic mechanism, the spin Hall conductivity is insensitive to scattering, i.e., impurities and disorder, when the carrier scattering time is sufficiently long. In contrast to this moderately dirty regime, in the dirty regime where the carrier scattering time is short, the spin Hall conductivity decreases with decreasing scattering time since the carrier scattering time limits the interband excitation that governs the intrinsic spin Hall effect [42]. The variation of the spin Hall effect in Pt studied previously is consistent with this scenario. However, although the intrinsic contribution depends on the Berry curvature of the band structure, as well as the carrier lifetime, the impact of the structural parameters, such as the lattice constant, on the spin Hall effect is still unclear.

In this paper, we demonstrate the robustness of the intrinsic spin Hall effect in Pt against the change in the lattice constant. We find that the spin Hall angle, the ratio of the spin Hall conductivity to the electric conductivity, of Pt is enhanced about 3 times by incorporating nitrogen atoms, which are dispersed in the Pt as interstitial impurities [43]. We observe that although the nitrogen incorporation changes the lattice constant of the Pt by a few percent, the variation of the intrinsic spin Hall conductivity induced by the nitrogen incorporation is consistent with the prediction of the crossover of the intrinsic spin Hall effect from the moderately dirty regime to the dirty-metal regime in Pt.

II. EXPERIMENTAL METHOD

We study the spin Hall effect in Pt films with different lattice constants and resistivities using spin-torque ferromagnetic resonance (ST-FMR). The structure of the devices is,

*ando@appi.keio.ac.jp

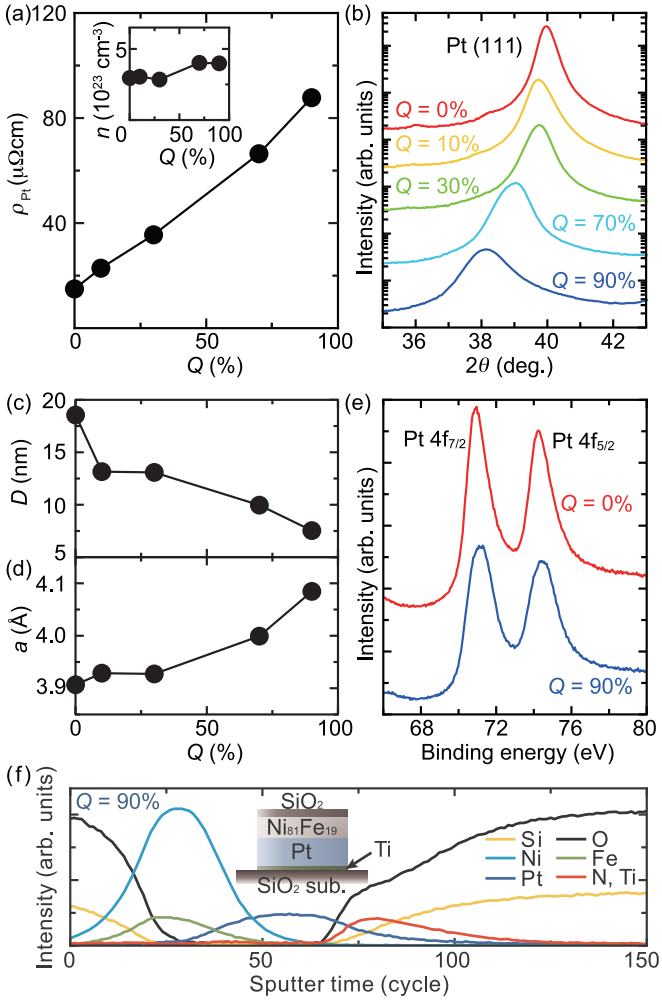

FIG. 1. (a) Q dependence of the electric resistivity ρ_{Pt} of the Pt layer. The inset shows the Q dependence of the carrier density n of the Pt layer, determined by Hall measurements. (b) x-ray diffraction patterns for the Pt single-layer films with different Q. The Q dependence of (c) the crystalline size D and (d) the lattice constant a of the Pt films, obtained from the XRD spectra. (e) The XPS spectra for the Pt single-layer films with $Q = 0\%$ and 90%. (f) The AES depth profile of the SiO_2-substrate/Ti(2)/Pt(7)/$Ni_{81}Fe_{19}$(5)/SiO_2(4) film with $Q = 90\%$. The inset shows the schematic illustration of the device.

from the substrate side, Ti(2)/Pt(7)/$Ni_{81}Fe_{19}$(5)/SiO_2(4). The numbers in parentheses represent the thickness in units of nanometers. The films were deposited on thermally oxidized Si substrates using magnetron sputtering. For the sputtering of the Pt layers, we introduced a mixture of argon and nitrogen gases into the chamber, where the relative nitrogen flow rate Q was varied.

The Pt films, sputtered with the mixture of argon and nitrogen gases, allow us to investigate the spin Hall effect by varying the lattice constant and resistivity. To investigate the characteristics of Pt with nitrogen incorporation, we prepared the Pt films sputtered with different Q on the Ti seed layers, where the sheet resistance of the Ti layers was confirmed to be orders of magnitude larger than that of the Pt layers. Figure 1(a) shows the electric resistivity ρ_{Pt} of the Pt layer with different Q. This result shows that ρ_{Pt} increases with Q monotonically. The increase of ρ_{Pt} with Q can be attributed to the decrease of the carrier scattering time with Q because the carrier density is almost unchanged by Q, as shown in the inset in Fig. 1(a).

To investigate the microstructure of the Pt films, we performed x-ray diffraction (XRD) measurements on the Pt films. As shown in Fig. 1(b), a strong (111) peak is observed, indicating a highly (111)-oriented texture in the Pt film. We note a broadening of the XRD peak, which indicates a reduction of the crystallite size with the increase of Q. From the full width at half maximum of the (111) diffraction and the Debye-Scherrer equation, we calculated the average crystallite size D, as shown in Fig. 1(c). Figure 1(c) shows that the crystallite size decreases by about 60% as Q is increased from 0% to 90%. Figure 1(b) also shows that the diffraction peak, at $2\theta = 39.97°$ for $Q = 0\%$, shifts towards lower angles with increasing Q, indicating an increase of the lattice constant. We show the lattice constant, calculated from the (111) diffraction peak position, in Fig. 1(d). This result shows that the lattice constant increases from 3.907 to 4.085 Å as Q is increased from 0% to 90%. The increase in the lattice constant of Pt with the nitrogen incorporation is consistent with a previous study [43]. The chemical states of Pt in the films were also investigated using x-ray photoelectron spectroscopy (XPS), as shown in Fig. 1(e). The Pt $4f_{7/2}$ binding energy for $Q = 0\%$ is 70.96 eV. The shift of the Pt $4f_{7/2}$ peak due to the change in Q is less than 0.2 eV. This result indicates that the nitrogen atoms exist as interstitial impurities, characterized by a very limited metal to nonmetal charge transfer [43,44].

To estimate the concentration of the nitrogen atoms in the Pt layer, we performed Auger electron spectroscopy (AES) combined with the Ar-ion sputtering. Figure 1(f) shows the AES depth profile of SiO_2-substrate/Ti(2)/Pt(7)/$Ni_{81}Fe_{19}$(5)/SiO_2(4) with $Q = 90\%$. Due to the fact that the nitrogen Auger peak overlaps the Ti Auger peak [45] and the Pt subpeak in Auger electron spectra, we show the intensity profile, instead of the atomic concentration, over the whole depth range. Assuming that Ti is absent in the Pt layer, we estimated the nitrogen concentration in the Pt layer after removing the contribution of the Pt subpeak. The nitrogen concentration in the Pt layer was determined to be 0.0, 8.7, and 10.0 at. % for $Q = 0\%$, 70%, and 90%, respectively. The AES result also shows a slight accumulation of nitrogen atoms near the Pt/$Ni_{81}Fe_{19}$ interface in the film with $Q = 90\%$. The driving force of the nitrogen accumulation can be attributed to the larger energetic stability of the $Ni_{81}Fe_{19}$ nitride than that of the interstitial nitrogen compounds in the Pt lattice. We confirmed that the nitrogen accumulation at the Pt/$Ni_{81}Fe_{19}$ interface is negligible when $Q \leqslant 70\%$, suggesting that the accumulation near the interface can be attributed to excess nitrogen atoms in the Pt lattice when $Q = 90\%$. We note that the slight accumulation of nitrogen atoms near the interface when $Q = 90\%$ plays a minor role in the generation of the spin-orbit torques, as discussed in the next section.

To study the spin Hall effect in the Pt films with the different lattice constants, the Pt/$Ni_{81}Fe_{19}$ films were patterned into rectangular bars with a width of 16 μm and a length of

120 μm using photolithography and Ar-ion etching. For the ST-FMR measurement, we applied an rf current with a frequency of f along the longitudinal direction of the device and swept an in-plane external field H applied at an angle of 45° from the longitudinal direction. The applied rf current induces oscillating torques on the magnetization in the $Ni_{81}Fe_{19}$ layer, causing the magnetization to precess at the FMR condition. The magnetization precession yields resistance oscillations due to the anisotropic magnetoresistance of $Ni_{81}Fe_{19}$. The change in the resistance mixes with the alternating current to create a DC voltage V_{DC} across the bar. We measured V_{DC} using a bias tee at room temperature.

III. RESULTS AND DISCUSSION

Figure 2(a) shows the ST-FMR spectra for the $Pt/Ni_{81}Fe_{19}$ bilayer with $Q = 90\%$. The resonance field H_{FMR} changes systematically with f, consistent with the prediction of the ST-FMR. The spectral shape of the ST-FMR signal changes with Q, as shown in Fig. 2(b). Figure 2(b) also shows the ST-FMR spectrum for the reference film $Ti(2)/Ni_{81}Fe_{19}(5)/SiO_2(4)$. The magnitude of the voltage for the reference film is negligibly small compared to that for the $Pt/Ni_{81}Fe_{19}$ bilayer films. The measured H dependence of V_{DC} can be decomposed into two components [17]:

$$V_{DC} = A\frac{W(\mu_0 H - \mu_0 H_{FMR})}{(\mu_0 H - \mu_0 H_{FMR})^2 + W^2} + S\frac{W^2}{(\mu_0 H - \mu_0 H_{FMR})^2 + W^2}, \quad (1)$$

where W is the spectral width. The symmetric S and antisymmetric A components are produced by the current-induced out-of-plane and in-plane effective fields, respectively. The out-of-plane field corresponds to the dampinglike effective field, while the in-plane effective field is the sum of the Oersted field and fieldlike effective field.

In a $Pt/Ni_{81}Fe_{19}$ bilayer with $Q = 0$, the fieldlike effective field is known to be negligibly small, compared to the dampinglike effective field and the Oersted field [46,47], and the spin-orbit torque in this system has been shown to be dominated by the bulk spin Hall effect in the Pt layer [35,39]. In the scenario of the bulk spin Hall effect, the dampinglike and fieldlike torques are approximately proportional to the real and imaginary parts of the spin mixing conductance, $\mathrm{Re}[G^{\uparrow\downarrow}]$ and $\mathrm{Im}[G^{\uparrow\downarrow}]$, respectively [48]. The negligible fieldlike torque in the $Pt/Ni_{81}Fe_{19}$ bilayer with $Q = 0$ is consistent with the expectation for metallic interfaces, where $\mathrm{Re}[G^{\uparrow\downarrow}] \gg \mathrm{Im}[G^{\uparrow\downarrow}]$ [49]. By changing Q, the fieldlike torque in the $Pt/Ni_{81}Fe_{19}$ bilayer can be non-negligible if the nitrogen incorporation enhances the interfacial spin-orbit coupling. The reason for this is that the interfacial spin-orbit coupling is the major source of the fieldlike torque through the Rashba-Edelstein effect and also that, in the scenario of the spin Hall effect, sizable $\mathrm{Im}[G^{\uparrow\downarrow}]$, or the fieldlike torque, can appear when a spin current reflected at the interface experiences a large angle rotation of its spin direction due to the interfacial spin-orbit coupling [50]. Because of this, the fieldlike torque has been found to be correlated with macroscopic quantities associated with the interfacial spin-orbit coupling, such as the interface perpendicular magnetic anisotropy energy density K_s and magnetic damping constant α [26].

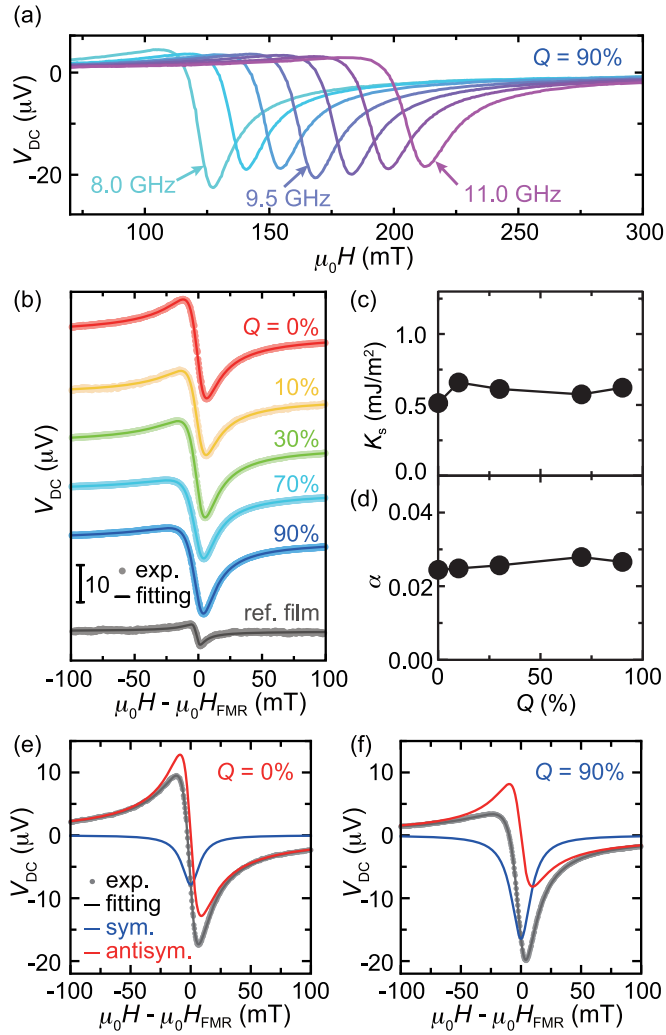

FIG. 2. (a) Magnetic field H dependence of the DC voltage V_{DC} for the $Pt/Ni_{81}Fe_{19}$ films with $Q = 90\%$ measured with an rf power of 20.0 dBm. The rf frequency was varied from $f = 8$ to 11 GHz. (b) V_{DC} spectra at $f = 10$ GHz for the $Pt/Ni_{81}Fe_{19}$ films with various Q and the reference film $Ti(2)/Ni_{81}Fe_{19}(5)/SiO_2(4)$. (c) Q dependence of the magnetic damping constant α for the $Pt/Ni_{81}Fe_{19}$ films. (d) Q dependence of the interface perpendicular magnetic anisotropy energy density K_s for the $Pt/Ni_{81}Fe_{19}$ films. The symmetric and antisymmetric components of the fitting results at $f = 10$ GHz for the $Pt/Ni_{81}Fe_{19}$ films with (e) $Q = 0\%$ and (f) $Q = 90\%$.

To test the role of the interfacial spin-orbit coupling in the $Pt/Ni_{81}Fe_{19}$ bilayers with different Q, we determined the Q dependence of the interface perpendicular magnetic anisotropy energy density K_s, which arises from the interfacial spin-orbit coupling [51,52]. We show the Q dependence of K_s in Fig. 2(c). This result was obtained from the values of H_{FMR}, determined from the ST-FMR signals, with the Kittel formula $2\pi f/\gamma = \sqrt{\mu_0 H_{FMR}(\mu_0 H_{FMR} + \mu_0 M_{eff})}$ and $M_{eff} = M_s - 2K_s/(\mu_0 M_s d_{FM})$ [53], where γ, M_s, M_{eff}, and d_{FM} are the gyromagnetic ratio, the saturation magnetization, the effective demagnetization field, and the thickness of the $Ni_{81}Fe_{19}$ layer, respectively. Figure 2(c) shows that K_s is

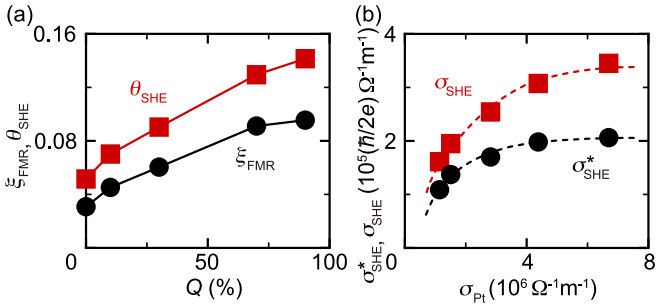

FIG. 3. The FMR spin-torque efficiency ξ_{FMR} (black circles) and the spin Hall angle $\theta_{SHE} = \xi_{FMR}/T_{int}$ (red squares) for the $Pt/Ni_{81}Fe_{19}$ films as a function of Q. (b) The spin Hall conductivity $\sigma_{SHE} = (\hbar/2e)\theta_{SHE}\sigma_{Pt}$ (red squares) and the effective spin Hall conductivity $\sigma^*_{SHE} = T_{int}\sigma_{SHE}$ (black circles) for the $Pt/Ni_{81}Fe_{19}$ films with different Q as a function of the electric conductivity σ_{Pt} of the Pt layer. The dotted curves are guides for eyes.

almost independent of Q, suggesting that the interfacial spin-orbit coupling is barely enhanced by the change in Q. The absence of an enhancement of the interfacial spin-orbit coupling with Q is supported by the magnetic damping constant α. In Fig. 2(d), we show the Q dependence of α, determined using $W = W_0 + (2\pi\alpha/\gamma)f$, where W_0 is the inhomogeneous linewidth. This result shows that α is independent of Q. The negligible change in α demonstrates that the interfacial spin-orbit coupling is barely enhanced by the change in Q because α is enhanced due to the interfacial spin memory loss (SML) when the interfacial spin-orbit coupling plays an important role [54]. These results indicate that a possible enhancement of the interfacial spin-orbit coupling can be neglected even in the $Q = 90\%$ device with the small accumulation of nitrogen atoms near the $Pt/Ni_{81}Fe_{19}$ interface, as well as in the devices with $Q \leqslant 70\%$ with the negligible nitrogen accumulation.

The absence of an enhancement of the interfacial spin-orbit coupling, evidenced by K_s and α, suggests that the spin-orbit torque in all the $Pt/Ni_{81}Fe_{19}$ bilayers with various Q is dominated by the spin Hall effect in the Pt layer. We note that the absence of a sizable interfacial spin-orbit coupling, which is the source of the fieldlike torque, allows us to assume that the in-plane effective field in the $Pt/Ni_{81}Fe_{19}$ films with various Q is dominated by the Oersted field produced by the current flow in the Pt layer. Under this assumption, the FMR spin-torque efficiency, defined as

$$\xi_{FMR} = \frac{S}{A}\frac{e\mu_0 M_s d_{FM} d_{Pt}}{\hbar}\sqrt{1 + \frac{M_{eff}}{H_{FMR}}}, \quad (2)$$

is related to the spin Hall angle θ_{SHE} of the Pt layer as $\xi_{FMR} = T_{int}\theta_{SHE}$, where d_{Pt} is the thickness of the Pt layer and T_{int} is the interfacial spin transparency [17]. In Figs. 2(e) and 2(f), we show the symmetric and antisymmetric components of the ST-FMR spectra, extracted by fitting the measured V_{DC} using Eq. (1), for the $Pt/Ni_{81}Fe_{19}$ films with $Q = 0\%$ and 90%. This result demonstrates that S/A, or ξ_{FMR}, is clearly enhanced by the nitrogen incorporation.

Figure 3(a) demonstrates that the effective spin Hall angle ξ_{FMR} increases with increasing Q. To extract the spin Hall angle θ_{SHE} from this result, we assume that the spin backflow dominates the reduction of the interfacial spin transparency in the $Pt/Ni_{81}Fe_{19}$ films; we neglect the reduction of the spin transparency due to the SML at the interface. This assumption is supported by the fact that the SML increases linearly with K_s of the interface [52] and K_s for the $Pt/Ni_{81}Fe_{19}$ films is small compared to the sample with a substantial SML [52]. The interfacial spin transparency set by the spin backflow with $G^{\uparrow\downarrow} \approx \mathrm{Re}[G^{\uparrow\downarrow}] \gg \mathrm{Im}[G^{\uparrow\downarrow}]$ is expressed as [31]

$$T_{int} = [1 - \mathrm{sech}(d_{Pt}/\lambda_s)]\left(1 + \frac{\tanh(d_{Pt}/\lambda_s)}{2\lambda_s\rho_{Pt}G^{\uparrow\downarrow}}\right)^{-1}, \quad (3)$$

where λ_s and σ_{Pt} are the spin diffusion length and the conductivity of the Pt layer, respectively. Here, we estimated λ_s for Pt with different Q from the measured values of σ_{Pt} by assuming a dominant role of the Elliott-Yafet spin relaxation mechanism ($\lambda_s \propto \sigma_{Pt}$) [29] and $\lambda_s = 1.4$ nm for Pt with $Q = 0$ [55,56]. The spin-mixing conductance $G^{\uparrow\downarrow}$ is related to the effective spin-mixing conductance $G^{\uparrow\downarrow}_{eff}$ as $G^{\uparrow\downarrow} = (\sigma_{Pt}/2\lambda_s)G^{\uparrow\downarrow}_{eff}/[\sigma_{Pt}/2\lambda_s - G^{\uparrow\downarrow}_{eff}\coth(d_{Pt}/\lambda_s)]$ [57,58], where the effective spin-mixing conductance $G^{\uparrow\downarrow}_{eff}$ can be determined experimentally using [57,58]

$$g^{\uparrow\downarrow}_{eff} = \frac{4\pi M_s d_{FM}}{\gamma\hbar}(\alpha - \alpha_0). \quad (4)$$

Here, $g^{\uparrow\downarrow}_{eff} \equiv G^{\uparrow\downarrow}_{eff}(h/e^2)$. Using the intrinsic magnetic damping constant of the $Ni_{81}Fe_{19}$ layer $\alpha_0 = 0.0092$, determined using the reference film $Ti(2)/Ni_{81}Fe_{19}(5)/SiO_2(4)$, we estimated T_{int} and extracted θ_{SHE} for the $Pt/Ni_{81}Fe_{19}$ films with different Q, as shown in Fig. 3(a).

We found that the spin Hall angle θ_{SHE} of the Pt layer is enhanced by about 3 times by increasing Q, as shown in Fig. 3(a). To understand the origin of the enhancement of the spin Hall angle, we plot the spin Hall conductivity $\sigma_{SHE} = (\hbar/2e)\theta_{SHE}\sigma_{Pt}$ and the effective spin Hall conductivity $\sigma^*_{SHE} = T_{int}\sigma_{SHE}$ with respect to the electric conductivity σ_{Pt} of the Pt layer, as shown in Fig. 3(b). This result shows that σ_{SHE} and σ^*_{SHE} decrease slowly in the higher-conductivity regime, then more quickly in the lower-conductivity regime with decreasing σ_{Pt}.

The variation of the spin Hall conductivity, shown in Fig. 3(b), is consistent with the prediction of the crossover of the intrinsic spin Hall effect from the moderately dirty regime to the dirty-metal regime. The spin Hall effect arises from intrinsic and extrinsic mechanisms [11,42,59–64]. The intrinsic contribution dominates the spin Hall conductivity of Pt in the moderately dirty and dirty-metal regimes where the carrier lifetime is short, whereas the extrinsic contributions are important only in the ultraclean regime where the carrier lifetime is very long [65]. The range of the conductivity of the Pt films used in the present study corresponds to the moderately dirty and dirty-metal regimes, where the intrinsic mechanism dominates the spin Hall effect. In Pt, the strong spin-orbit coupling lifts the double degeneracy of the d bands. The intrinsic spin Hall effect originates from the interband transitions between these bands [28]. In the moderately dirty regime, where the carrier lifetime τ is sufficiently long, the intrinsic spin Hall conductivity is almost independent of the electric conductivity, $\sigma_{xx} \propto \tau$. In contrast, in the dirty-metal regime, the interband excitation is governed by τ, and the

intrinsic spin Hall conductivity decreases with decreasing σ_{xx} [42,66]. As shown in Fig. 3(b), the observed variation of σ_{SHE} for the Pt films is consistent with this scenario. A recent theoretical study showed that mechanical deformations of Pt can change the intrinsic spin Hall conductivity due to the change in the splitting of the near-degenerate states [67]. The calculation indicates that the spin Hall conductivity is not significantly changed by a few percent change in the lattice constant. The observation of the crossover of the intrinsic spin Hall effect under the variation of the lattice constant is consistent with this calculation.

IV. CONCLUSIONS

In summary, we have investigated the spin Hall effect in Pt against the change in the lattice constant. The lattice constant of the Pt film was varied by a few percent through the nitrogen incorporation without a significant change in the chemical states. We found that the spin Hall angle is enhanced by a factor of 3 as the resistivity of the Pt film is increased by the nitrogen incorporation. The variation of the spin Hall effect is consistent with the prediction of the crossover of the intrinsic spin Hall effect from the moderately dirty regime to the dirty-metal regime. This observation indicates that the variation of the intrinsic spin Hall conductivity in Pt is dominated by the change in the scattering time, rather than a change in the band structure, under a few percent change in the lattice constant.

ACKNOWLEDGMENTS

This work was supported by JSPS KAKENHI Grants No. 19H00864, No. 20H00337, No. 19K22131, and No. 20H02593; the Canon Foundation; the Asahi Glass Foundation; and the Spintronics Research Network of Japan (Spin-RNJ).

[1] M. I. Dyakonov and V. Perel, Phys. Lett. A **35**, 459 (1971).
[2] J. E. Hirsch, Phys. Rev. Lett. **83**, 1834 (1999).
[3] Y. Kato, R. Myers, A. Gossard, and D. Awschalom, Science **306**, 1910 (2004).
[4] J. Wunderlich, B. Kaestner, J. Sinova, and T. Jungwirth, Phys. Rev. Lett. **94**, 047204 (2005).
[5] E. Saitoh, M. Ueda, H. Miyajima, and G. Tatara, Appl. Phys. Lett. **88**, 182509 (2006).
[6] S. O. Valenzuela and M. Tinkham, Nature (London) **442**, 176 (2006).
[7] T. Kimura, Y. Otani, T. Sato, S. Takahashi, and S. Maekawa, Phys. Rev. Lett. **98**, 156601 (2007).
[8] K. Uchida, S. Takahashi, K. Harii, J. Ieda, W. Koshibae, K. Ando, S. Maekawa, and E. Saitoh, Nature (London) **455**, 778 (2008).
[9] H. Nakayama, M. Althammer, Y.-T. Chen, K. Uchida, Y. Kajiwara, D. Kikuchi, T. Ohtani, S. Geprägs, M. Opel, S. Takahashi, R. Gross, G. E. W. Bauer, S. T. B. Goennenwein, and E. Saitoh, Phys. Rev. Lett. **110**, 206601 (2013).
[10] A. Hoffmann, IEEE Trans. Magn. **49**, 5172 (2013).
[11] J. Sinova, S. O. Valenzuela, J. Wunderlich, C. H. Back, and T. Jungwirth, Rev. Mod. Phys. **87**, 1213 (2015).
[12] K. Ando, S. Takahashi, K. Harii, K. Sasage, J. Ieda, S. Maekawa, and E. Saitoh, Phys. Rev. Lett. **101**, 036601 (2008).
[13] I. M. Miron, K. Garello, G. Gaudin, P.-J. Zermatten, M. V. Costache, S. Auffret, S. Bandiera, B. Rodmacq, A. Schuhl, and P. Gambardella, Nature (London) **476**, 189 (2011).
[14] L. Liu, C.-F. Pai, Y. Li, H. Tseng, D. Ralph, and R. Buhrman, Science **336**, 555 (2012).
[15] A. Manchon, J. Železny, I. M. Miron, T. Jungwirth, J. Sinova, A. Thiaville, K. Garello, and P. Gambardella, Rev. Mod. Phys. **91**, 035004 (2019).
[16] C. O. Avci, A. Quindeau, C.-F. Pai, M. Mann, L. Caretta, A. S. Tang, M. C. Onbasli, C. A. Ross, and G. S. Beach, Nat. Mater. **16**, 309 (2017).
[17] L. Liu, T. Moriyama, D. C. Ralph, and R. A. Buhrman, Phys. Rev. Lett. **106**, 036601 (2011).
[18] A. V. Khvalkovskiy, V. Cros, D. Apalkov, V. Nikitin, M. Krounbi, K. A. Zvezdin, A. Anane, J. Grollier, and A. Fert, Phys. Rev. B **87**, 020402(R) (2013).
[19] J. Kim, J. Sinha, M. Hayashi, M. Yamanouchi, S. Fukami, T. Suzuki, S. Mitani, and H. Ohno, Nat. Mater. **12**, 240 (2013).
[20] X. Qiu, K. Narayanapillai, Y. Wu, P. Deorani, D.-H. Yang, W.-S. Noh, J.-H. Park, K.-J. Lee, H.-W. Lee, and H. Yang, Nat. Nanotechnol. **10**, 333 (2015).
[21] J. Yoon, S.-W. Lee, J. H. Kwon, J. M. Lee, J. Son, X. Qiu, K.-J. Lee, and H. Yang, Sci. Adv. **3**, e1603099 (2017).
[22] S. Fukami, C. Zhang, S. DuttaGupta, A. Kurenkov, and H. Ohno, Nat. Mater. **15**, 535 (2016).
[23] H. An, Y. Kageyama, Y. Kanno, N. Enishi, and K. Ando, Nat. Commun. **7**, 13069 (2016).
[24] H. Nakayama, Y. Kanno, H. An, T. Tashiro, S. Haku, A. Nomura, and K. Ando, Phys. Rev. Lett. **117**, 116602 (2016).
[25] T. Gao, A. Qaiumzadeh, H. An, A. Musha, Y. Kageyama, J. Shi, and K. Ando, Phys. Rev. Lett. **121**, 017202 (2018).
[26] Y. Kageyama, Y. Tazaki, H. An, T. Harumoto, T. Gao, J. Shi, and K. Ando, Sci. Adv. **5**, eaax4278 (2019).
[27] H. An, Y. Kanno, A. Asami, and K. Ando, Phys. Rev. B **98**, 014401 (2018).
[28] G. Y. Guo, S. Murakami, T.-W. Chen, and N. Nagaosa, Phys. Rev. Lett. **100**, 096401 (2008).
[29] E. Sagasta, Y. Omori, M. Isasa, M. Gradhand, L. E. Hueso, Y. Niimi, Y. Otani, and F. Casanova, Phys. Rev. B **94**, 060412 (2016).
[30] R. Ramaswamy, Y. Wang, M. Elyasi, M. Motapothula, T. Venkatesan, X. Qiu, and H. Yang, Phys. Rev. Appl. **8**, 024034 (2017).
[31] M.-H. Nguyen, D. C. Ralph, and R. A. Buhrman, Phys. Rev. Lett. **116**, 126601 (2016).
[32] L. Zhu and R. A. Buhrman, Phys. Rev. Appl. **12**, 051002(R) (2019).
[33] X. Zhou, M. Tang, X. L. Fan, X. P. Qiu, and S. M. Zhou, Phys. Rev. B **94**, 144427 (2016).
[34] M. Obstbaum, M. Decker, A. K. Greitner, M. Haertinger, T. N. G. Meier, M. Kronseder, K. Chadova, S. Wimmer,

D. Ködderitzsch, H. Ebert, and C. H. Back, Phys. Rev. Lett. **117**, 167204 (2016).
[35] L. Zhu, D. C. Ralph, and R. A. Buhrman, Phys. Rev. Appl. **10**, 031001(R) (2018).
[36] L. Zhu, K. Sobotkiewich, X. Ma, X. Li, D. C. Ralph, and R. A. Buhrman, Adv. Funct. Mater. **29**, 1805822 (2019).
[37] M.-H. Nguyen, M. Zhao, D. Ralph, and R. Buhrman, Appl. Phys. Lett. **108**, 242407 (2016).
[38] U. Shashank, R. Medwal, T. Shibata, R. Nongjai, J. V. Vas, M. Duchamp, K. Asokan, R. S. Rawat, H. Asada, S. Gupta, and Y. Fukuma, Adv. Quantum Technol. **4**, 2000112 (2021).
[39] L. Zhu, L. Zhu, M. Sui, D. C. Ralph, and R. A. Buhrman, Sci. Adv. **5**, eaav8025 (2019).
[40] J. W. Lee, Y.-W. Oh, S.-Y. Park, A. I. Figueroa, G. van der Laan, G. Go, K.-J. Lee, and B.-G. Park, Phys. Rev. B **96**, 064405(R) (2017).
[41] H. Hayashi, A. Musha, H. Sakimura, and K. Ando, Phys. Rev. Research **3**, 013042 (2021).
[42] T. Tanaka, H. Kontani, M. Naito, T. Naito, D. S. Hirashima, K. Yamada, and J. Inoue, Phys. Rev. B **77**, 165117 (2008).
[43] T. Harumoto, T. Sannomiya, S. Muraishi, J. Shi, and Y. Nakamura, J. Appl. Crystallogr. **47**, 1490 (2014).
[44] A. Hecq, J. Delrue, M. Hecq, and T. Robert, J. Mater. Sci. **16**, 407 (1981).
[45] P. Dawson and K. Tzatzov, Surf. Sci. **149**, 105 (1985).
[46] H. An, T. Ohno, Y. Kanno, Y. Kageyama, Y. Monnai, H. Maki, J. Shi, and K. Ando, Sci. Adv. **4**, eaar2250 (2018).
[47] S. Haku, A. Musha, T. Gao, and K. Ando, Phys. Rev. B **102**, 024405 (2020).
[48] V. P. Amin and M. D. Stiles, Phys. Rev. B **94**, 104420 (2016).
[49] M. Zwierzycki, Y. Tserkovnyak, P. J. Kelly, A. Brataas, and G. E. W. Bauer, Phys. Rev. B **71**, 064420 (2005).
[50] J. Kim, J. Sinha, S. Mitani, M. Hayashi, S. Takahashi, S. Maekawa, M. Yamanouchi, and H. Ohno, Phys. Rev. B **89**, 174424 (2014).
[51] H. X. Yang, M. Chshiev, B. Dieny, J. H. Lee, A. Manchon, and K. H. Shin, Phys. Rev. B **84**, 054401 (2011).
[52] L. Zhu, D. C. Ralph, and R. A. Buhrman, Phys. Rev. Lett. **122**, 077201 (2019).
[53] V. Tshitoyan, C. Ciccarelli, A. P. Mihai, M. Ali, A. C. Irvine, T. A. Moore, T. Jungwirth, and A. J. Ferguson, Phys. Rev. B **92**, 214406 (2015).
[54] J.-C. Rojas-Sánchez, N. Reyren, P. Laczkowski, W. Savero, J.-P. Attané, C. Deranlot, M. Jamet, J.-M. George, L. Vila, and H. Jaffrès, Phys. Rev. Lett. **112**, 106602 (2014).
[55] W. Zhang, W. Han, X. Jiang, S.-H. Yang, and S. S. Parkin, Nat. Phys. **11**, 496 (2015).
[56] L. Liu, R. Buhrman, and D. Ralph, arXiv:1111.3702.
[57] Y. Tserkovnyak, A. Brataas, and G. E. W. Bauer, Phys. Rev. B **66**, 224403 (2002).
[58] H. J. Jiao and G. E. W. Bauer, Phys. Rev. Lett. **110**, 217602 (2013).
[59] R. Karplus and J. Luttinger, Phys. Rev. **95**, 1154 (1954).
[60] J. Sinova, D. Culcer, Q. Niu, N. A. Sinitsyn, T. Jungwirth, and A. H. MacDonald, Phys. Rev. Lett. **92**, 126603 (2004).
[61] S. Murakami, N. Nagaosa, and S. C. Zhang, Science **301**, 1348 (2003).
[62] J. Smit, Physica (Amsterdam) **24**, 39 (1958).
[63] L. Berger, Phys. Rev. B **2**, 4559 (1970).
[64] M. Gradhand, D. V. Fedorov, P. Zahn, and I. Mertig, Phys. Rev. Lett. **104**, 186403 (2010).
[65] G. Vignale, J. Supercond. Novel Magn. **23**, 3 (2010).
[66] H. Kontani, M. Naito, D. S. Hirashima, K. Yamada, and J.-I. Inoue, J. Phys. Soc. Jpn. **76**, 103702 (2007).
[67] Y. He, Y. Ji, and W. Zhang, Phys. B (Amsterdam, Neth.) **605**, 412654 (2021).